EES Batteries

Accepted Manuscript

This article can be cited before page numbers have been issued, to do this please use: H. Yang, H. Liu, J. Zhang, T. Zhang, X. Zhu, Z. Liu, L. Zhu, C. C. Cao, G. Xu and M. Zhu, *EES Batteries*, 2025, DOI: 10.1039/D5EB00085H.

View Article Online
DOI: 10.1039/D5EB00085H

Broader context statement

Lithium-sulfur (Li-S) batteries are considered one of the most promising next-generation battery technologies due to their high theoretical energy density, which have the advantages of low cost and high capacity, but the cathode shuttle effect and the growth of anode lithium dendrites have hindered development. Among the various modification strategies, nanofiber composite separator modification offers a promising approach to address issues on both anodes and cathodes. Here, an innovative approach by combined ultrathin poly [2, 6-diimidazo (4,5-b:4',5'-e) pyridinylene-1,4(2,5-dihydroxy) phenylen] (PIPD) nanofiber coating (1 μm) with polypropylene (PP) matrix to develop a functional separator (PP@PIPD). Benefiting from high dipole moment (stronger molecular polarity contrary to alkyls groups), PIPD enables excess electrons promoting the decomposition of LiTFSI and generate LiF, thus forming a stable solid electrolyte interface (SEI). In addition, polysulfides precipitation kinetics were accelerated by promoting the desolvation of Li^+. This work elucidates the critical impact of Li^+ desolvation on high-rate Li-S batteries. The batteries with PP@PIPD separator possessed superior competitiveness in terms of average capacity fading, initial capability, coulombic efficiency and long-term cyclability, compared with the reported separators for Li-S batteries, demonstrating promising prospects for developing Li-S batteries.

View Article Online
DOI: 10.1039/D5EB00085H

Enhancing Lithium-Ion Desolvation with Robust Polyhydroquinone-Diimidazopyridine Nanofibers for High-Rate Li-S Batteries

Hao Yang[1]†, Haoyu Liu[1]†, Jia Zhang[1]†, Tao Zhang[1], Xiaoqing Zhu[1], Zhongxiu Liu[1], Liping Zhu[1]*, Changyong (Chase) Cao[2], Guiyin Xu[1]*, Meifang Zhu[1]

[1]*State Key Laboratory of Advanced Fiber Materials, College of Materials Science and Engineering, Donghua University, Shanghai 201620, China*

[2]*Laboratory for Soft Machines & Electronics, Department of Mechanical and Aerospace Engineering, Case Western Reserve University, Cleveland, OH 44106, USA*

†These authors contribute equally to this paper.

Corresponding Authors: zhulp@dhu.edu.cn; xuguiyin@dhu.edu.cn

Abstract

Lithium-sulfur (Li-S) batteries have attracted considerable attention based on their high energy density. Nevertheless, the shuttle effect of lithium polysulfide (LiPS) and the growth of lithium dendrite remain primary issues hindering their commercial application. Herein, a novel functional separator based on polypropylene (PP) matrix was proposed, modified with an ultrathin poly[2,6-diimidazo(4,5-b:4',5'-e)pyridinylene-1,4(2,5-dihydroxy)phenylene] (PIPD) nanofibers layer via a scalable blade-coating process. Compared to unmodified PP, PIPD-coated separator demonstrates significantly enhanced mechanical strength. The PIPD nanofiber coating demonstrates superior lithiophilicity, effectively reducing lithium-ion desolvation energy barrier while enhancing deposition kinetics, thereby promoting the formation of uniform lithium nucleation sites. Additionally, the imidazole groups in PIPD act as Lewis acids, notably adsorbing Lewis-based LiPSs and mitigating the shuttle effect. Consequently, Li||Li cells assembled with modified separators demonstrated stable cycling over 1,800 hours at 1 mA cm^{-2}/1 mAh cm^{-2}. Remarkably, Li-S batteries demonstrated a specific capacity retention of 728.9 mAh g^{-1} after 450 cycles at 3C, with an ultralow capacity fade rate of only 0.072% per cycle. The proposed innovative strategy enhances the performance and safety of Li-S batteries while paving the way for their commercial viability in advanced energy storage applications.

Keywords: Lithium-sulfur batteries, Lithium dendrite, Lithium-ion desolvation,

View Article Online
DOI: 10.1039/D5EB00085H

Functionalized separator, Nanofiber coating

Introduction

The expanding requirements for energy storage infrastructure, driven by accelerating adoption of renewable energy generation and electric mobility, mandate technological breakthroughs in next-generation battery systems.[1, 2] Li-S batteries have garnered extensive attention owing to their theoretical energy density of 2600 Wh kg^{-1}, outperforming to that of conventional lithium-ion batteries.[3] However, the commercialization of Li-S batteries confronts severe hurdles, mainly affected by the shuttle effect of polysulfides and slow redox kinetics for sulfur, which collectively result in the rapid capacity deterioration.[4] Moreover, the shuttle of LiPSs compromises the structural integrity of the solid electrolyte interphase (SEI), accelerating lithium dendrite growth and posing critical safety concerns.[5] The key to addressing these challenges lies in optimizing the reaction kinetics of LiPSs and stabilizing the SEI, which is critical for the commercial application of Li-S batteries.

Various strategies have been proposed to mitigate these issues, focusing on sulfur host optimization using conductive carbon or porous materials to anchor LiPSs,[6, 7] the introduction of catalysts aimed at improving sulfur reaction kinetics,[8] and the introduction of functional electrolytes to stabilize the SEI.[9] Despite these efforts, the practical application of Li-S batteries remains constrained by slow conversion kinetics of LiPSs and instability of SEI. The separator serves as an important component, of which performance directly effects the cycle stability of battery systems.[10] Conventional polyolefin-based separators (polypropylene (PP) and polyethylene (PE)),

View Article Online
DOI: 10.1039/D5EB00085H

fail to suppress dendritic growth and polysulfide shuttle, due to their large, uneven pores and non-polar nature.[11]

Recent researches have highlighted the potential of modifying commercial separators with functional coatings to address these limitations. Various coatings, including organic polymers (e.g., cellulose derivatives,[12, 13] polybenzimidazole,[14, 15] polyimides[16, 17]), inorganic materials (e.g., transition metal phosphides,[18, 19] carbon materials,[20] ceramic materials[21]), and organic-inorganic composites (e.g., metal-organic frameworks[22]), have been explored. Among these, poly[2,6-diimidazo(4,5-b:4',5'-e)pyridinylene-1,4(2,5-dihydroxy)phenylene] (PIPD) represents a uniquely promising candidate due to its molecular structure. The rigid-rod polymer backbone with extended π-conjugation provides exceptional mechanical stability, while its ortho-positioned hydroxyl groups create polar domains that could facilitate lithium-ion coordination.[23, 24] Simultaneously, the electron-deficient imidazole rings in PIPD's heterocyclic units offer potential Lewis acid sites for polysulfide interaction.[25] This combination of structural robustness, polar characteristic, and chemical affinity enables PIPD to function as a multifunctional separator material that simultaneously addresses both dendrite growth and polysulfide shuttle—a dual function rarely achieved by conventional coating materials.

Herein, we developed an ultrathin functional separator with abundant lithophilic sites, uniformly distributed electric field, and strong interactions with LiPSs. Fabricated by blade-coating PP substrates with a 1 μm layer of PIPD nanofibers, the functional separator exhibits remarkable mechanical properties, achieving nearly double the tensile strength (91 MPa) of uncoated PP separators. The abundant nitrogen atoms and hydroxyl groups in the PIPD structure promote lithium-ion desolvation by the formation of instantaneous bonds to generate homogeneous lithium nucleation sites, thus enabling dendrite-free lithium deposition. The modification mechanism was

View Article Online
DOI: 10.1039/D5EB00085H

elucidated using in situ optical microscopy and molecular dynamics simulations. Additionally, the positively charged imidazole groups in PIPD serve as Lewis acids, effectively immobilizing LiPSs and accelerating reaction kinetics. Consequently, Li||Cu cells assembled with PP@PIPD separators achieve a coulombic efficiency (CE) of 99.5% over 1000 cycles at 1 mA cm^{-2}. Moreover, Li-S batteries assembled with PP@PIPD delivered a specific capacity of 728.9 mAh g^{-1} over 450 cycles at 3C.

Results and Discussion

PIPD nanofibers (PIPDNF) were prepared from micro-sized PIPD fibers *via* a sol-gel conversion method.[26] Micrometer-sized PIPD fibers were dissolved in a homogeneous trifluoroacetic acid (TFA)/methanesulfonic acid (MSA) mixture, where strong acids protonated nitrogen and oxygen atoms on the PIPD main chain, weakening intermolecular forces and enabling the fibers to exfoliation into nanofibers (Figure 1a). This transformation reduced the fiber diameter from 800 μm to approximately 100 nm (Figure 1b; Figure S1, Supplementary Information). The X-ray diffraction (XRD) profile reveals distinct Bragg diffraction peaks at 2θ = 10.5°, 20°, and 27.5°, related to the (200), (110), and (110) planes of PIPDNF, respectively (Figure 1d).[27, 28] The peaks were broader and less intense compared to PIPD microfibers (PIPDMF), confirming the successful conversion to nanofibers.[28] The chemical structure of PIPD fibers was characterized by Fourier transform infrared spectroscopy (FTIR), with absorption peaks at 2920 cm^{-1} attributed to secondary amino groups.[29] Notably, the nanofibers exhibit significant broadening of the hydroxyl stretching vibration peak within the 3200-3600

View Article Online
DOI: 10.1039/D5EB00085H

cm^{-1}, indicating an increased number of free hydroxyl groups on the surface. This phenomenon originates from nanoscale effect-induced changes in molecular chain orientation, resulting in an enhanced density of hydrogen-bonding networks among phenolic hydroxyl groups (Figure 1e).[30, 31] The increase in hydrogen bonding is attributed to the random nanofiber network structure. Table S1 (Supplementary Information) presents a systematic analysis of characteristic peak assignments, while X-ray photoelectron spectroscopy (XPS) results confirm the elemental composition of PIPDNF, with distinct peaks for O 1s, N 1s, and C 1s (Figure S2, Supplementary Information).[32] The C 1s spectra revealed peaks corresponding to C=N, C-C, C-N, and C-O, corroborating the structure of PIPDNF (Figure 1f).[29] The comprehensive experimental characterization results conclusively demonstrate the successful synthesis of PIPDNF.

The PIPDNF slurry was uniformly coated with a specific thickness onto commercial PP (Celgard 2400) separators using a scalable blade-coating technique, followed by aging in an isopropyl alcohol (IPA) bath (Figure 1c). During aging, IPA functioned as a Bronsted acid, promoting phase separation through proton removal from solvated PIPDNF. Raman spectroscopy revealed that the characteristic peaks of PP@PIPD separator retained similar vibration features characteristic of PIPDNF, despite slight intensity reduction, confirming chemical structural preservation during coating (Figure 1g). The key peaks at 1642, 1505, 1371, and 1313 cm^{-1} represent benzene ring vibrations, -C=N-, and C=C stretching.[33]

View Article Online
DOI: 10.1039/D5EB00085H

The tensile strength of PP@PIPD separator, with a 1 μm PIPDNF coating (Figure S3, Supplementary Information), was significantly elevated to 91 MPa, compared to 44 MPa for the pristine PP separator. The performance enhancement originates from the three-dimensional hydrogen-bonding network formed by hydroxyl (-OH) and imino (-NH-) groups within the nanofiber architecture (Figure 1h; Figure S4, Supplementary Information)[27]. This tensile strength surpasses most previously reported values, highlighting the material's potential for large-scale applications (Figure 1i).[34-43] Thermal stability is crucial for battery safety in commercial applications. While PP separators exhibited significant shrinkage at 155°C, PP@PIPD separator showed no deformation under similar conditions (Figure S5, Supplementary Information), due to the intrinsic synergistic interactions within the PIPD nanofiber coating. Despite its ultrathin nature, the PIPD coating mechanically reinforces the separator to redistribute thermal stresses and restrict molecular mobility in the PP substrate. Additionally, the robust interfacial bonding at the PIPD and PP interface establishes a structurally integrated composite system, where the coating stabilizes the substrate by inhibiting polymer chain relaxation under heat. The high thermal resistance of PIPD further enhances this effect by acting as a thermal barrier, reducing heat transfer to the PP substrate and mitigating deformation. Together, these factors transform the separator into a composite structure with significantly improved thermal stability, effectively suppressing the shrinkage of the PP substrate. In addition, the poor compatibility of traditional polyolefin separators with polar electrolytes is a significant limitation in lithium-ion transport.[44, 45] Contact angle (CA) measurements demonstrate improved

View Article Online
DOI: 10.1039/D5EB00085H

wettability of PP@PIPD separator (CA = 13°) compared to the pristine PP separator (CA = 52°), which originates from the increased surface exposure of -OH and -NH- functional groups on the PIPD polymer framework (Figure S7, Supplementary Information).[46]

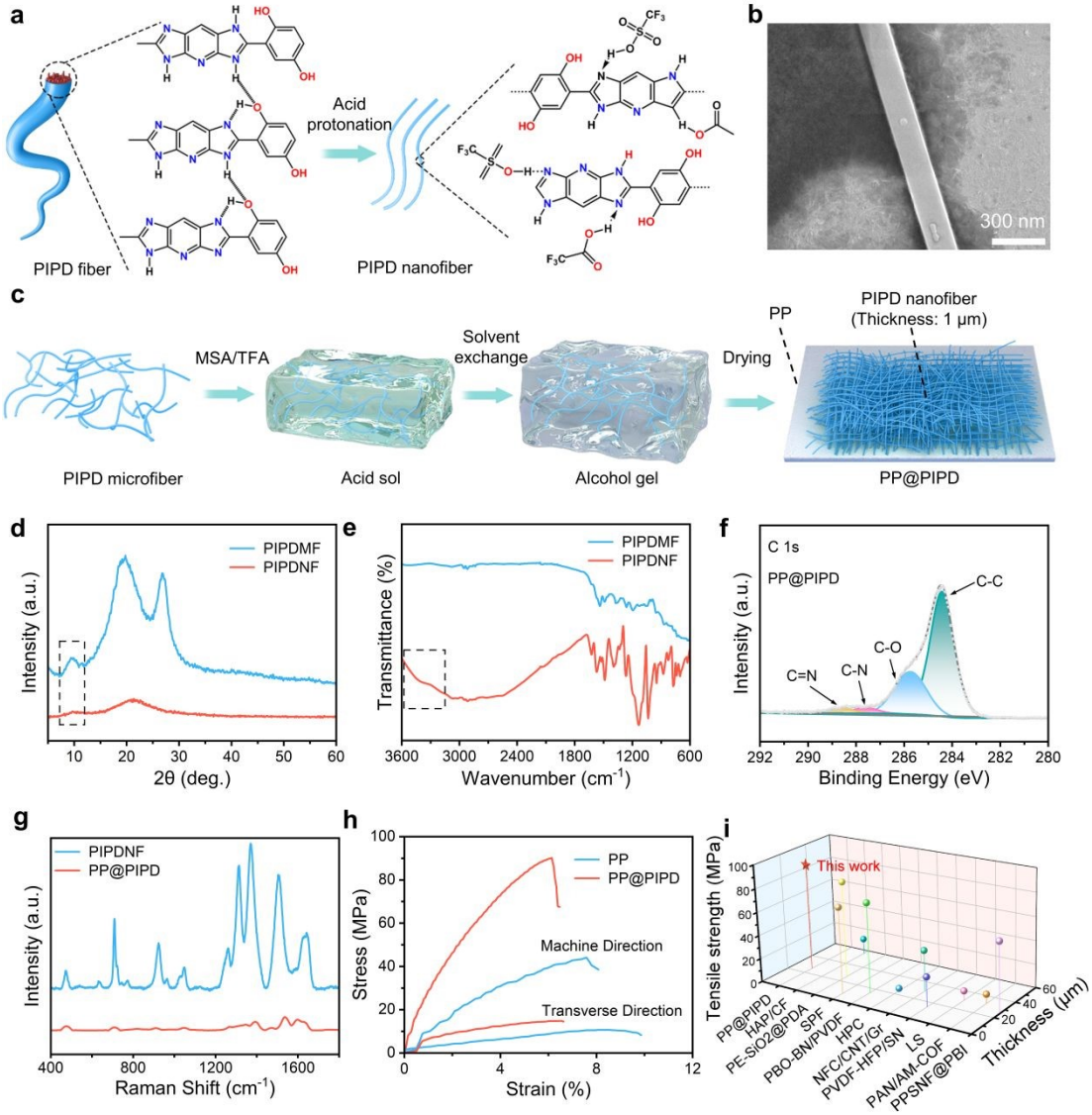

Figure 1. Fabrication and Characteristic of PP@PIPD Separators. (a) Preparation illustration of PIPDNF via MSA/TFA treating. (b) The SEM image of PIPDNF. (c) Schematic of the preparation process for PP@PIPD. (d) XRD of PIPDMF and PIPDNF. (e) FTIR spectra of PIPDMF and PIPDNF. (f) XPS spectra for C 1s of PP@PIPD separator. (g) Raman spectra of PIPDNF and PP@PIPD separators. (h) Stress-strain curves (transverse and machine directions) of separators. (i) Comparison of machine tensile strength for PP@PIPD and other coated separators.

View Article Online
DOI: 10.1039/D5EB00085H

To elucidate the regulatory mechanism of separator-induced interfacial effect on the dynamic evolution of Li^+ solvation structures, classical molecular dynamics (MD) simulations were performed at the separator-electrolyte interface, with the representative configuration of Simulation depicted in Figure 2a-b. Radial distribution functions (RDFs) reveal that the peaks for Li^+-O ($TFSI^-$) are located at 1.91 Å and 1.93 Å for the PP and PP@PIPD separator systems, respectively, indicating a slight increase in the average distance for coordinated species in the PP@PIPD system (Figures 2c-d). The stretch of Li^+-O ($TFSI^-$) bonds originates from PIPD's hydroxyl groups competitively coordinating with Li^+ (Li^+-O distance: 1.97 Å), which partially displaces $TFSI^-$ anions from the primary solvation shell. Notably, two peaks associating to Li^+-N (PIPD) and Li^+-O (PIPD) emerge at 1.93 Å and 1.97 Å in the PP@PIPD system, demonstrating that PIPD impacts the solvation structure of Li^+ despite its moderate Li^+ affinity. The imidazole nitrogen atoms further change the solvation environment through Lewis acid-base interactions, absorbing electron density from coordinated solvent molecules and reducing their binding strength with Li^+. The interaction between PIPD and Li^+ weakens the coordination between Li^+ and electrolyte components, resulting in a comparable bulk desolvation energy barrier of ~8.01 eV for both PP and PP@PIPD separators. However, at the interface, PP separator shows a higher desolvation energy (6.88 eV) than PP@PIPD separator (4.89 eV), indicating that PP@PIPD separator facilitates Li^+ desolvation. This interface advantage stems from the synergistic effect of PIPD, where hydroxyl induced solvation shell changes reduce Li^+ desolvation energy, while imidazole induced charge redistribution weakens the

View Article Online
DOI: 10.1039/D5EB00085H

interaction between lithium ions and solvents. The decrease in activation energy in Li||Li cells assembled with PP@PIPD separators compared to those assembled with PP provides additional experimental validation of the phenomenon (Figure 2e; Figure S8, Supplementary Information).

Density functional theory (DFT) calculations were systematically conducted between PIPD and LiPSs to investigate the chemical interactions mechanisms (Figure 2f). PIPD exhibits higher binding energies with Li_2S_8, Li_2S_6, Li_2S_4, Li_2S_2, and Li_2S (-1.44, -1.27, -1.5, -2.07, and -2.1 eV, respectively) compared to the bare PP (-0.31, -0.67, -0.59, -0.62, and -0.46 eV). These results confirm the superiority of PIPD to capture LiPSs, attributed to the electron-deficient imidazole groups, which exhibit strong adsorption capability. Consistent with these findings, the H-type glass cell experiments show reduced polysulfide permeability in the presence of PP@PIPD separator (Figure S9, Supplementary Information).

View Article Online
DOI: 10.1039/D5EB00085H

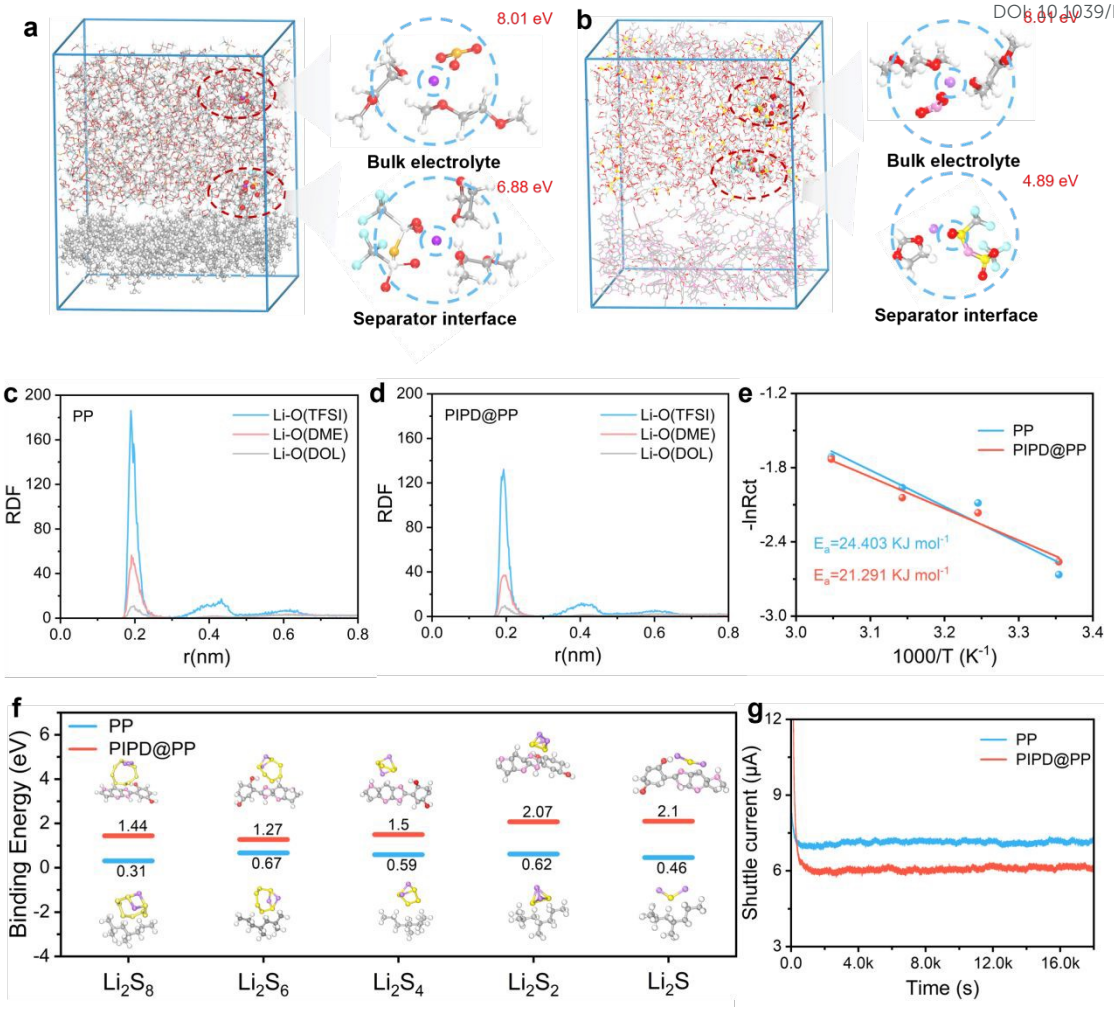

Figure 2. Lithium-Ion Desolvation and Interaction between PIPD and LiPSs. (a, b) MD simulation snapshots and lithium-ion desolvation energy for bulk electrolyte and separator interfaces in PP and PP@PIPD separator systems, respectively. (c, d) Radial distribution function (RDF) of Li^+ in PP and PP@PIPD separator systems. (e) Activation energy for Li^+ transport in Li||Li cells. (f) Binding energy of PP and PP@PIPD separators with various Li_2S_x species (x= 1, 2, 4, 6, and 8). (g) Shuttle current.

Quantitative evaluation of polysulfide shuttle suppression was conducted through shuttle current measurements, revealing that cells with conventional PP separators exhibited a 23.6% higher shuttle current (7.3 μA) compared with the PP@PIPD (5.9 μA) (Figure 2g). The effective shuttle suppression enhances the cycling stability and electrochemical performance, demonstrating the unique superiority of PP@PIPD separator.

View Article Online
DOI: 10.1039/D5EB00085H

A systematic investigation of lithium-ion transference number (t_{Li^+}) and ionic conductivity was performed to elucidate the influence of reduced desolvation energy on ions transport. The results demonstrate that PP@PIPD separator enables a significant higher ionic conductivity, markedly exceeding that of the pristine PP separators (Figure S10, Supplementary Information). Similarly, the t_{Li^+} value of PP@PIPD separator (0.72) was substantially higher than PP separator (0.4) (Figure 3a; Figure S11, Supplementary Information). Experimental results demonstrate that PP@PIPD separator significantly enhances the diffusion kinetics of lithium-ion flux while optimizing its spatial distribution uniformity, thereby effectively improving the overall electrochemical performance.[47] Coulombic efficiency (CE) was measured to quantify Li plating/stripping behavior. The results demonstrate that PP@PIPD separator maintains a stable CE of 99.5% over 1000 cycles (1 mA cm^{-2}/1 mAh cm^{-2}). Instead, the cells using PP separators displayed a significant drop in CE after just 100 cycles (Figure 3b). The nucleation overpotential (μ_n) in Li||Cu cells were systematically evaluated to elucidate the influence of the separators on Li deposition kinetics (Figure 3c). The cells using PP@PIPD separator exhibited a significantly lower μ_n value of 27 mV, which is 3.6 times smaller than the 99 mV observed for the cells using PP separator. In situ optical microscopy was conducted to dynamically track real-time lithium dendrite growth in optically accessible Li symmetric cells under galvanostatic plating at 12.5 mA cm^{-2} (Figure S12, Supplementary Information). Prior to electrochemical cycling, distinct physical separation between the separator and lithium anode was observed. After 10 minutes of plating, a porous and loosely packed lithium deposition

View Article Online
DOI: 10.1039/D5EB00085H

layer formed on Li surface when using PP separator. By 30 minutes, the gap between PP separator and lithium foil was filled with severe lithium dendrites. In contrast, the PP@PIPD composite separator system exhibited a planar lithium deposition morphology with uniform crystallographic orientation, while maintaining observable interfacial separation between the modified separator assembly and metallic lithium anode throughout prolonged electrochemical cycling (Figure S13, Supplementary Information).

Li symmetric cells equipped with PP@PIPD separator showed a stable polarization voltage (13 mV) (Figure 3d). In contrast, the cells using PP separators demonstrated a markedly higher overpotential (1 mA cm^{-2}/1 mA cm^{-2}), thus deteriorating cycling performance. Remarkably, the cells with PP@PIPD separators maintained a lower polarization voltage at 1 mAh cm^{-2} across a broad current density range (1-5 mA cm^{-2}), implying superior electrochemical stability (Figure 3e). Electrochemical impedance spectroscopy (EIS) measurements further confirm that Li||Li cells using PP@PIPD separators possess a reduced interfacial resistance compared to those using PP separator (Figure S14, Supplementary Information). These results highlight the superior cycling stability of lithium-ion/metal batteries using PP@PIPD separator, surpassing most previously reported results in the literature (Figure 3f).[26, 34, 48-51] The performance enhancement is based on the inherent capability of PIPD nanofibers to regulate Li^+ deposition behavior, forming a flat and compact Li plating layer. The effectiveness of PP@PIPD separator was further confirmed by the deposition morphology of metallic lithium in Li symmetric cells after 25 cycles

View Article Online
DOI: 10.1039/D5EB00085H

assembled with various separators (Figure S15, Supplementary Information).

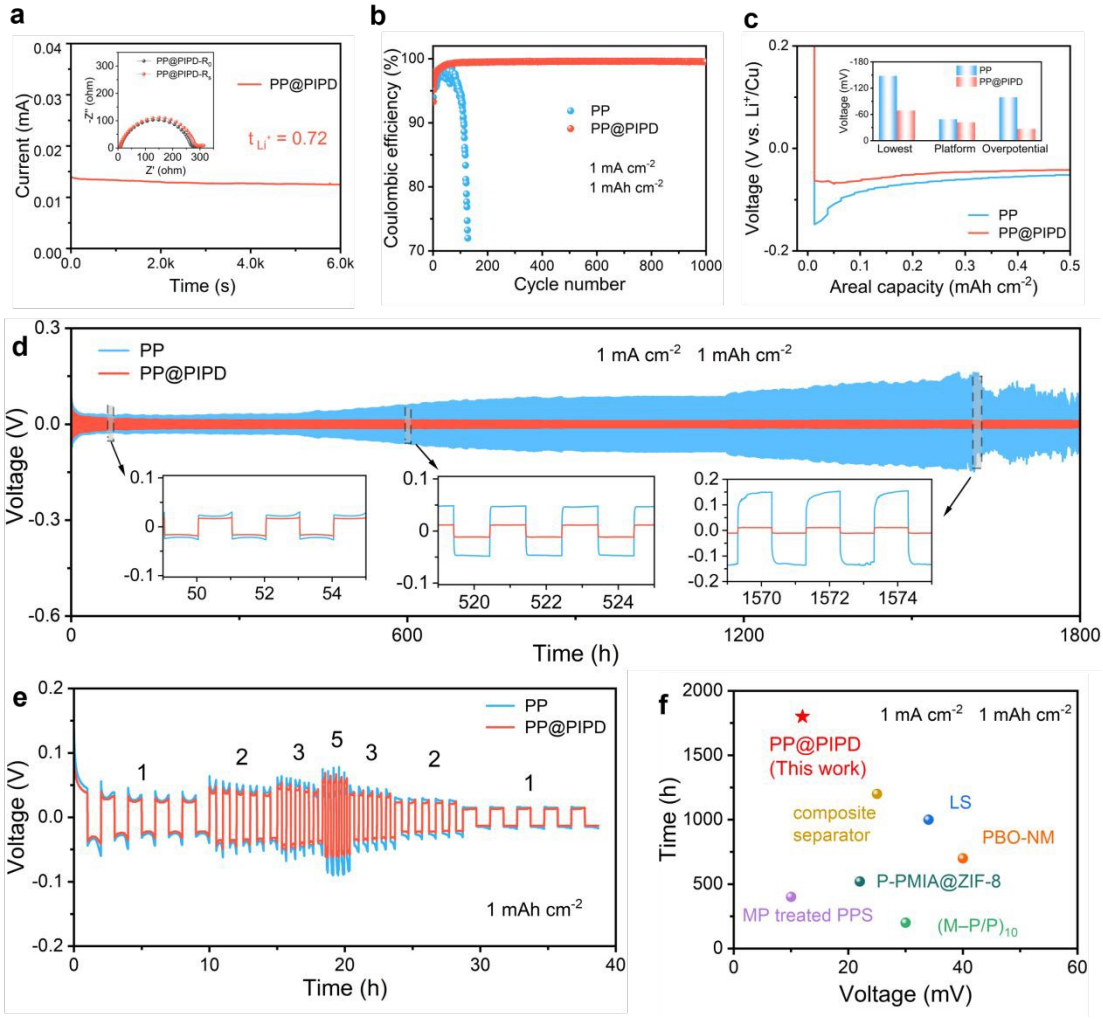

Figure 3. Electrochemical Performance of Cells Assembled with Various Separators. (a) Chronoamperometric response of Li||Li cells using PP@PIPD separators (Inset: Nyquist plots). (b) CE profiles. (c) Nucleation overpotential in Li||Li cells. (d) Voltage-time profiles and (e) Rate performance for Li||Li cells. (f) Integrated Performance comparison between this paper and previously reported literatures.

Li plating/stripping process was investigated by cyclic voltammetry (CV) of Li||Cu cells (Figure 4a). The cells using PP@PIPD separators behaved markedly enhanced current response compared to PP separators, indicating improved lithium-ion transport and deposition behavior. To further analyze reaction kinetics, Tafel plots were recorded (Figure 4b). Li||Li cells using PP@PIPD separators exhibited an exchange current density (i_0) of 0.145 mA cm^{-2}, significantly surpassing that of the cells using PP

View Article Online
DOI: 10.1039/D5EB00085H

separators. This result is consistent with the observed enhancement in lithium-ion kinetics. EIS was measured on Li||Li cells with various separators to assess interfacial resistance (R_{int}) before and after being rested at 50°C for 24 hours. At room temperature, the cells with PP separators displayed a significantly higher R_{int} of 174.8 Ω compared to those utilizing PP@PIPD separator (115.3 Ω) (Figure 4c). After resting at 50°C for 24 hours, the R_{int} of cells with PP@PIPD separator showed only a slight increase (Figure 4d), confirming its substantially improved interfacial stability. The improved stability originates from the strong interfacial interaction between the PIPD nanofiber coating and lithium anode, which promotes uniform lithium deposition. XPS analysis of cycled Li anodes after three cycles reveals distinct SEI composition differences (Figure 4e). The SEI formed with PP separators exhibited substantial organic components, primarily Li-OR and Li-OC_2OR[52], indicative of electrolyte decomposition. Li anode with PP@PIPD separators exhibited a decreased proportion of organic components in comparison, indicating that PP@PIPD separator promotes efficient Li^+ desolvation and minimizes solvent-induced corrosion of Li anode. Furthermore, The SEI formed by PP@PIPD separator showed elevated LiF content (Figure 4f), which contributes to enhanced protection of Li anode and stabilize the SEI.

View Article Online
DOI: 10.1039/D5EB00085H

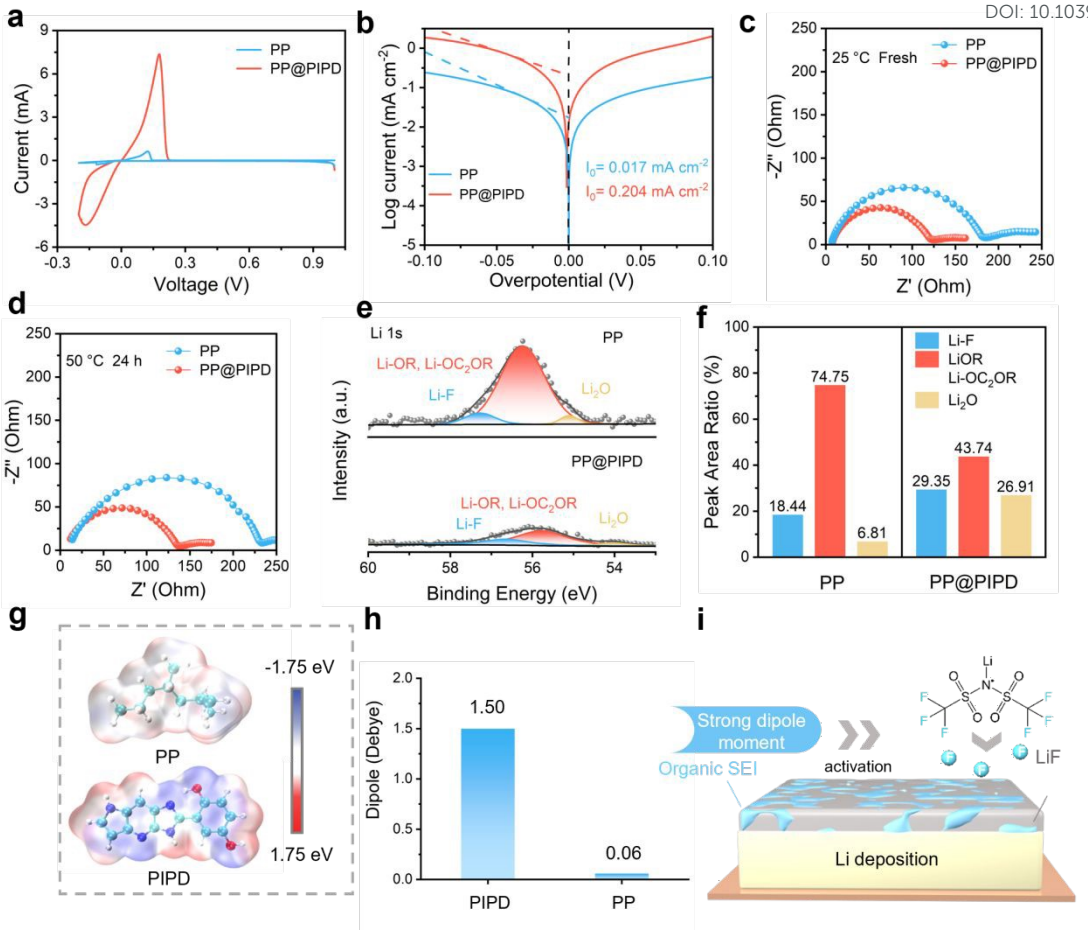

Figure 4. The Mechanism of SEI Formation. (a) The CV profiles of Li||Cu cells. (b) Tafel polarization profiles. Nyquist profiles of Li symmetric cells at (c) 25°C for fresh and (d) 50°C for 24 h. (e) XPS spectra for Li 1s of cycled lithium anodes. (f) Li content of SEI in Li symmetric cells. (g) Calculated ESP of PP and PIPD. (h) The dipole moment of PP and PIPD. (i) Schematic illustration of strong dipole moment's impact on the decomposition of LiTFSI for SEI formation.

To elucidate the role of PIPD in LiTFSI decomposition and LiF formation, DFT simulations were performed, including electrostatic potential (ESP) mapping (Figure 4g) and dipole moment calculations (Figure 4h). The ESP maps revealed regions of electrophilicity (red) and nucleophilicity (blue), indicating that the strong dipole moments of hydroxyl and nitrogen groups in PIPD promote electron transfer to the electrolyte. Compared to alkyl groups, the higher molecular polarity of PIPD facilitates the decomposition of LiTFSI, generating F^- species and forming substantial LiF in the

View Article Online
DOI: 10.1039/D5EB00085H

SEI (Figure 4i). In summary, PP@PIPD separator improves lithium-ion kinetics and stabilizes the SEI by promoting LiTFSI decomposition and enhancing the formation of LiF, which protects Li anode from degradation. The results demonstrate that PIPD is pivotal in enabling high-performance lithium metal batteries.

The LiPSs shuttle effect and sluggish reduction kinetics represent the primary obstacles to enhancing Li-S batteries performance. Wettability tests using Li_2S_6 electrolyte confirmed the strong adsorption interaction of PIPD with polysulfides. The Li_2S_6 electrolyte exhibited a contact angle (CA) of 21° on PP@PIPD separator, showing a markedly lower value compared to the 34° observed on the pristine PP separator, indicating superior wettability and stronger adsorption by PIPD (Figure 5a). Self-discharge testing was performed to elucidate the interfacial interactions between PIPD and LiPSs. After 20 cycles at 0.2C, the cells were charged to 2.8 V, rested for 72 h, and then cycled again for 20 cycles (Figure S17, Supplementary Information). During self-discharge, high-order polysulfides spontaneously convert to low-order polysulfides, causing a voltage drop.[53] Open-circuit voltage (OCV) monitoring during the relaxation period revealed that the cells with PP@PIPD composite separators showed a attenuated voltage decline compared to those with conventional PP separators, indicating reduced polysulfide migration and enhanced retention of active sulfur species (Figure 5b). Furthermore, the charge-discharge profiles reveal that batteries with PP@PIPD separators showed a reduced capacity loss compared to those with the conventional PP separator (Figure S18, Supplementary Information). Tafel corrosion tests assess the corrosion resistance of the separators. Li foil and stainless steel were employed as the

View Article Online
DOI: 10.1039/D5EB00085H

anode and cathode, respectively, with different electrolyte components tested on either side of the cells. The cells with PP@PIPD separator exhibited a more positive corrosion potential than PP separator (Figure 5c), suggesting that the parasitic reactions between Li anode and polysulfides were effectively suppressed. PP@PIPD separator facilitated faster Li^+ desolvation, promoting accelerated Li_2S deposition kinetics. To examine the liquid-solid conversion of LiPSs, chronoamperometric nucleation experiments were conducted by Li||Li_2S_8 cells with carbon paper as the cathode and 0.2 M Li_2S_8 catholyte as the active material. The *i*−*t* curves reveal three stages: reduction of soluble Li_2S_8 and Li_2S_6 (orange and grey) and nucleation of Li_2S (blue or red). The PP@PIPD-based cells demonstrated a significantly higher Li_2S nucleation capacity (162.96 mAh g^{-1}) compared to the PP-based cells (54.56 mAh g^{-1}). Additionally, the morphology of Li_2S deposition on carbon paper showed uniform nucleation size using PP@PIPD separator, which favors the stable cycling performance of the full batteries (Figures 5d-e). Electron-deficient imidazole groups in PIPD enhance polysulfide adsorption and facilitate rapid Li^+ desolvation. This dual effect not only enhances LiPSs immobilization but also accelerates their nucleation kinetics at the cathode/LiPSs interface, substantially boosting Li-S batteries discharge performance.

Galvanostatic intermittent titration technique (GITT) was employed to dynamically explore internal polarization during the discharge process. The PP@PIPD-assembled batteries exhibited a smaller working voltage drop, although both exhibited similar equilibrium voltages, indicating reduced polarization and faster cathode kinetics (Figure 5f). XPS analysis demonstrated a higher sulfur content in the SEI of PP

View Article Online
DOI: 10.1039/D5EB00085H

separator-based batteries (78%) compared to PP@PIPD separator system (61%), indicating more severe parasitic interactions between LiPSs and lithium metal anode in PP separator system (Figure 5g-i). Additionally, the proportion of F-containing species in the SEI formed with PP@PIPD separator revealed that LiF was the dominant fluoride component (37%), further demonstrating the protective role of PP@PIPD separator.

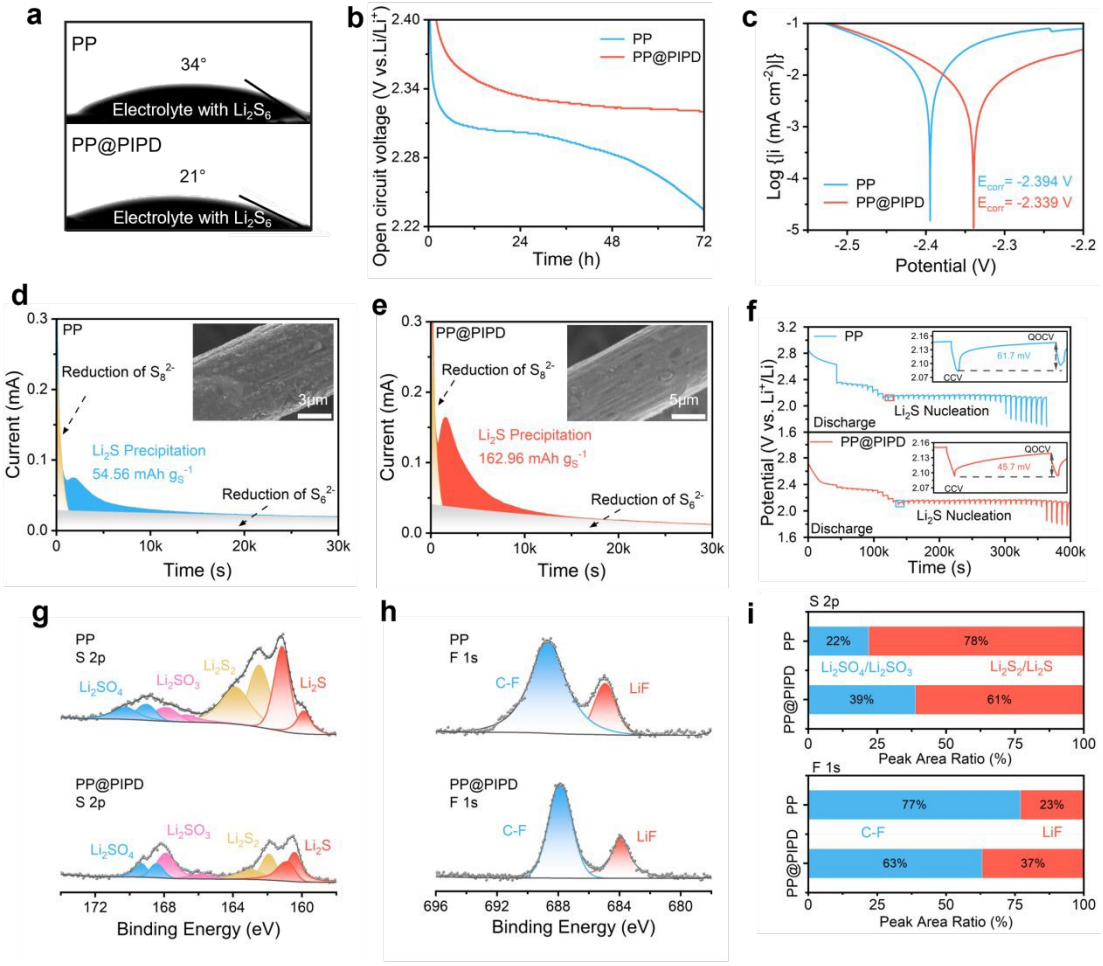

Figure 5. Evaluation on Shuttle Inhibition and Cathode Kinetics of LiPSs with Various Separators. (a) The contact angle measurements of 10 mM Li_2S_6-containing electrolytes. (b) The OCV records of Li-S batteries. (c) Potentiodynamic polarization profiles of Li symmetric cells. Chronoamperometric discharge response of full batteries assembled with (d) PP and (e) PP@PIPD separators at constant voltage (2.03 V). Inset: The morphology of Li_2S deposition on carbon papers. (f) GITT curves. XPS of (g) S 2p and (h) F 1s on cycled Li anodes (5 cycles). (i) S (upper) and F (below) content of the SEI.

View Article Online
DOI: 10.1039/D5EB00085H

The imidazole functional groups in PP@PIPD separator significantly enhance polysulfide adsorption to mitigate the shuttle effect while improving sulfur utilization efficiency. PP@PIPD separator effectively suppresses parasitic reactions and promotes homogeneous Li_2S deposition, which results in an improvement in the cycling stability of Li-S batteries, as evidenced by its superior performance over extended cycles. The CV profiles of Li-S batteries assembled with PP and PP@PIPD separators at (Figure 6a) displayed three distinct peaks: Peak A: Initial reduction of S_8 to long-chain Li_2S_x ($4 \leq x \leq 8$); Peak B: Subsequent conversion to solid-phase Li_2S_2/Li_2S, respectively. Conversely, Peak C corresponds to the oxidative reconversion process where Li_2S_2/Li_2S is electrochemically reverted to S_8.[54] The batteries assembled with PP@PIPD separators delivered higher peak intensity and reduced polarization in contrast to those using PP separators, suggesting that the deposition and reoxidation of Li_2S were significantly enhanced. Tafel analysis of Peak B showed a smaller slope for the PP@PIPD-based full cell (65.6 mV dec^{-1}) compared to the PP-based cell (165.6 mV dec^{-1}), further confirming enhanced Li_2S deposition kinetics (Figure 6b).

EIS analysis was performed to analyze reaction kinetics. The Nyquist plots of full batteries at 1C, both fresh and after 25 cycles, were characterized by a high-frequency semicircle related to charge transfer resistance (R_{ct}), and a linear Warburg impedance response in the low frequency region (Figure 6c; Figure S20, Supplementary Information).[55] The batteries with PP@PIPD separators showed significantly lower R_{ct} after 25 cycles, demonstrating improved charge transfer and sulfur species utilization compared to batteries with PP separators. The rate performance of Li-S batteries

View Article Online
DOI: 10.1039/D5EB00085H

equipped with PP@PIPD was compared with that of the batteries equipped with PP separators (Figure 6d). The specific discharge capacities of the batteries with PP@PIPD separators at 0.2, 0.5, 1, 3, and 5C were 1169.1, 921.7, 843.5, 707.7, and 592.3 mAh g^{-1}, respectively. Conversely, the batteries equipped with PP separators displayed lower capacities of 1074.8, 819.6, 739.4, 609.3, and 444.8 mAh g^{-1} under the same conditions. The lower overpotentials and higher capacity retention at various rates further highlights the advantages of PP@PIPD separator (Figure 6e; Figure S21, Supplementary Information).

The discharge profiles exhibited two distinct voltage plateaus reflecting the sequential phase transitions from S_8 to Li_2S_4 (Q_1) and subsequently from Li_2S_4 to Li_2S (Q_2). The batteries with PP@PIPD separators achieved higher Q_1 and Q_2 values, with a Q_2/Q_1 ratio closer to the theoretical value (3), indicating more complete sulfur conversion and higher sulfur utilization (Figure S22, Supplementary Information). The cycling stability of Li-S batteries assembled with PP@PIPD separators was systematically assessed at 3C. The cells maintained exceptional capacity retention over 450 cycles with near-100% CE (Figure 6g). At 0.2C, the cells with PP@PIPD separator displayed an initial specific capacity of 1093.8 mAh g^{-1} (CE ≈ 100%), maintaining 665.5 mAh g^{-1} after 100 charge-discharge cycles. Comparatively, the cells assembled with PP separator showed markedly inferior performance, sustaining 385.7 mAh g^{-1} with a significantly lower CE of 31.3% after same cycles (Figure 6h).

View Article Online
DOI: 10.1039/D5EB00085H

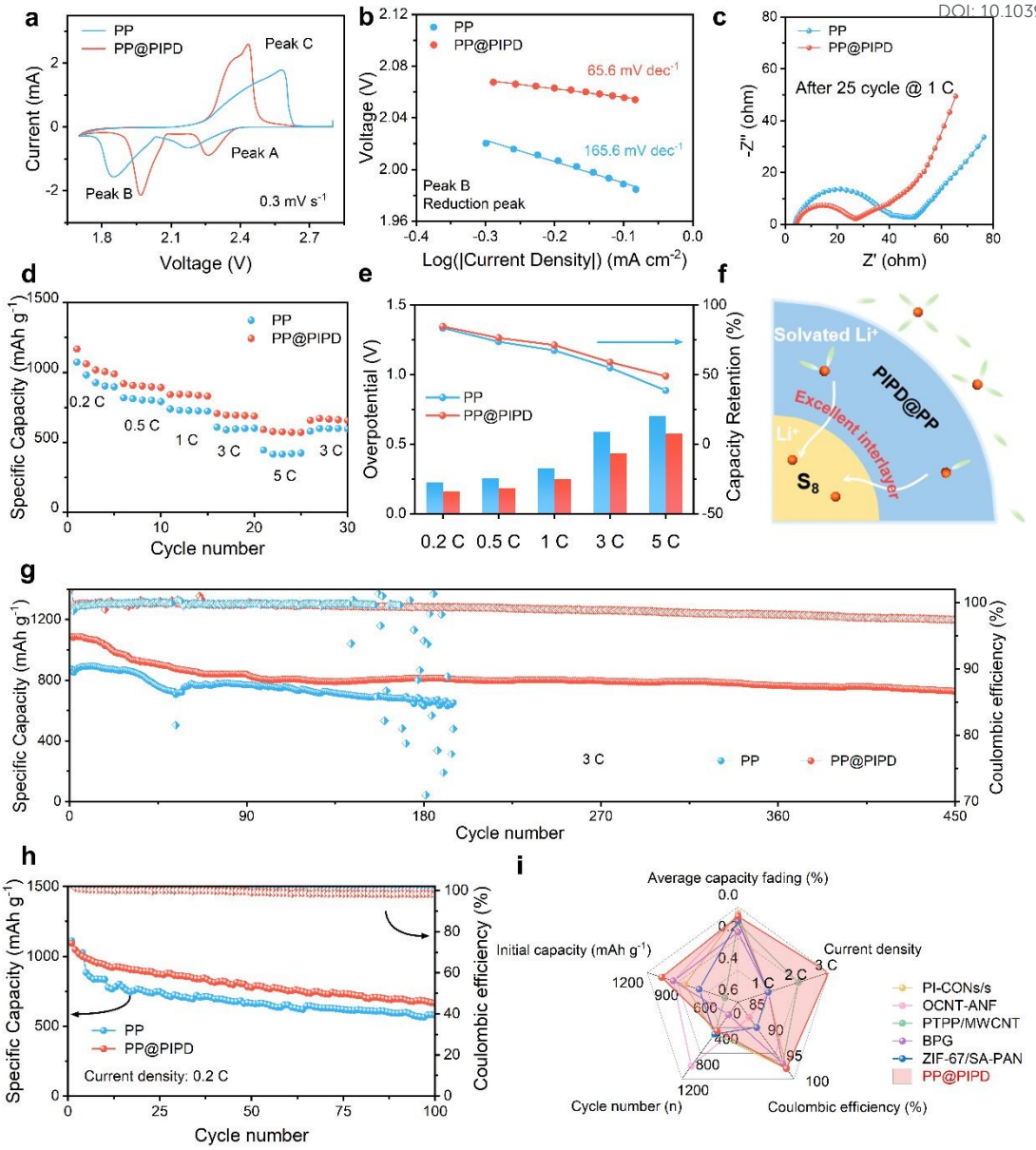

Figure 6. Electrochemical Characterization of Li-S Batteries Assembled with Various Separators. (a) CV profiles (0.3 mV s^{-1}). (b) Tafel polarization analysis from peak B. (c) Nyquist curves for Li-S batteries after 25 charge-discharge cycles at 1C. (d) Rate performance. (e) The overpotential and capacity retention profiles among different current densities. (f) Work mechanisms of multifunctional PP@PIPD separators. The cycling profiles of full batteries at (g) 3C and (h) 0.2C. (i) The comparison of integrated performance between this paper and other reported fiber-based separators in Li-S batteries.

The surface morphology of lithium anodes was observed after cycling (Figure S23, Supplementary Information). After 500 cycles at 0.2C, lithium anodes paired with PP separators showed significant cracking, likely due to reactions between polysulfides

View Article Online
DOI: 10.1039/D5EB00085H

and Li anode. In contrast, anodes paired with PP@PIPD separators remained flat and smooth. Even after 1000 cycles, Li anodes with PP@PIPD separators maintained a smooth surface (Figure S24, Supplementary Information). PP@PIPD separators demonstrate comprehensive performance advantages over existing temperature-resistant fibrous separators in Li-S batteries application, including significantly improved capacity retention, enhanced initial discharge capacity, near-theoretical CE, and superior cycle stability (Figure 6i).[56-60] The imidazole and hydroxyl groups in PIPD favor contribute to facilitating Li^+ desolvation, accelerating Li_2S precipitation, and stabilizing the sulfur utilization process.

Conclusion

In summary, the integration of PIPD coating onto polypropylene separator presents an effective strategy to tackle critical challenges in Li-S batteries, including dendritic lithium growth and the polysulfide shuttle effect. The N atoms and hydroxyl groups in PIPD form instantaneous bonds that accelerate lithium-ion desolvation, enabling rapid and uniform lithium deposition. Additionally, the Lewis-acidic imidazole groups in PIPD exhibit strong interactions with LiPSs, effectively suppressing the shuttle effect and enhancing sulfur utilization. PIPD-based separator demonstrated exceptional mechanical properties, achieving nearly double the tensile strength (91 MPa) of the uncoated PP separator with only a 1 μm PIPDNF coating. Electrochemical performance tests revealed remarkable stability and efficiency: PP@PIPD separator demonstrates exceptional electrochemical performance, enabling Li||Li cells to maintain stable

View Article Online
DOI: 10.1039/D5EB00085H

cycling for over 1800 hours at 1 mA cm^{-2}, Li||Cu cells to achieve a consistent 99.5% average Coulombic efficiency throughout 1000 cycles. Notably, Li-S full batteries showed superior cycling durability with merely 32.6% capacity fade after 450 cycles at 3C. These results confirm the considerable potential of PIPD-modified separators in improving the performance, safety, and cycle life of Li-S batteries, paving the way for their practical application in next-generation energy storage systems.

Author contributions

Xu, G. conducted the conceptual design, project management and resource support; **Xu, G.** and **Cao, C.** handled funding acquisition and guidance; **Yang, H.** carried out material preparation and electrochemical testing; **Liu, H.** provided material synthesis and analytical characterization; **Zhang, J.** performed theoretical computational simulations; **Yang, H., Liu, H**. and **Zhang, J.** drafted the manuscript; **Zhu, M., Zhu, L., Zhang, T., Zhu, X. and Liu, Z.** participated in the guidance and revision of the paper.

Conflicts of Interest

The authors declare no competing financial interests or personal relationships to disclose.

Acknowledgements

This paper was supported by National Key Research and Development Program of China (2022YFB3803502), National Natural Science Foundation of China (52103076, 52203005), Fundamental Research Funds for the Central Universities (2232025A-05), Interdisciplinary Frontier Innovation Team Development Special Fund of Donghua University, Shanghai Rising-Star Program (24QA2700100), the International Cooperation Fund of the Science and Technology Commission of Shanghai Municipality (24520713300), and the Joint Funds of the National Natural Science

View Article Online
DOI: 10.1039/D5EB00085H

Foundation of China (U23B2079). C.C. acknowledge the support from USDA-NIFA (2021-67021-42113) and Case Western Reserve University.

References

1. L. Cheng, J. Liu, H. Wang, Y. Guo, A. Shao, Y. Li, Z. Wang, Y. Zhang, J. Tang, C. Li and Y. Ma, A Lightweight, Li Supplementary and Lithiophilic Interface Enables Anode-Less Lithium Metal Battery Prototyping, *EES Batteries*, 2025, **1**(3), 555-565, DOI: 10.1039/D5EB00042D.
2. D. Larcher and J. M. Tarascon, Towards Greener and More Sustainable Batteries for Electrical Energy Storage, *Nat. Chem.*, 2015, **7**(1), 19-29, DOI: 10.1038/nchem.2085.
3. J. T. Frith, M. J. Lacey and U. Ulissi, A Non-Academic Perspective on the Future of Lithium-Based Batteries, *Nat. Commun.*, 2023, **14**(1), 420, DOI: 10.1038/s41467-023-35933-2.
4. Z. Shi, Z. Tian, D. Guo, Y. Wang, Z. Bayhan, A.S. Alzahrani and H.N. Alshareef, Kinetically Favorable Li–S Battery Electrolytes, *ACS Energy Lett.*, 2023, **8**(7), 3054-3080, DOI: 10.1021/acsenergylett.3c00826.
5. L. Wang, K. Yue, Q. Qiao, Z. Zhao, Y. Xu, L. Pan, Y. Liu, H. Li and B. Zhu, In Situ Self-Polymerization of Thioctic Acid Enabled Interphase Engineering Towards High-Performance Lithium–Sulfur Battery, *Adv. Energy Mater.*, 2025, **15**(1), 2402617, DOI: 10.1002/aenm.202402617.
6. H. Yuan, J. Zheng, G. Lu, L. Zhang, T. Yan, J. Luo, Y. Wang, Y. Liu, T. Guo, Z. Wang, J. Nai and X. Tao, Formation of 2D Amorphous Lithium Sulfide Enabled by Mo_2C Clusters Loaded Carbon Scaffold for High-Performance Lithium Sulfur Batteries, *Adv. Mater.*, 2024, **36**(28), 2400639, DOI: 10.1002/adma.202400639.
7. H. Chen, G. Zhou, D. Boyle, J. Wan, H. Wang, D. Lin, D. Mackanic, Z. Zhang, S. C. Kim, H. R. Lee, H. Wang, W. Huang, Y. Ye and Y. Cui, Electrode Design with Integration of High Tortuosity and Sulfur-Philicity for High-Performance Lithium-Sulfur Battery, *Matter*, 2020, **2**(6), 1605-1620, DOI: 10.1016/j.matt.2020.04.011.
8. M. Xu, Q. Zhu, Y. Li, Y. Gao, N. Sun and B. Xu, Atom-Dominated Relay Catalysis of High-Entropy MXene Promotes Cascade Polysulfide Conversion for Lithium–Sulfur Batteries, *Energy Environ. Sci.*, 2024, **17**(20), 7735-7748, DOI: 10.1039/d4ee03402c.
9. Y. Liu, L. Xu, Y. Yu, M. He, H. Zhang, Y. Tang, F. Xiong, S. Gao, A. Li, J. Wang, S. Xu, D. Aurbach, R. Zou and Q. Pang, Stabilized Li-S Batteries with Anti-Solvent-Tamed Quasi-Solid-State Reaction, *Joule*, 2023, **7**(9), 2074-2091, DOI: 10.1016/j.joule.2023.07.013.
10. M. Chen, M. Shao, J. Jin, L. Cui, H. Tu and X. Fu, Configurational and Structural Design of Separators toward Shuttling-Free and Dendrite-Free Lithium-Sulfur Batteries: A Review, *Energy Stor. Mater.*, 2022, **47**, 629-648, DOI: 10.1016/j.ensm.2022.02.051.
11. Z. Ju, J. Nai, Y. Wang, T. Liu, J. Zheng, H. Yuan, O. Sheng, C. Jin, W. Zhang, Z. Jin, H. Tian, Y. Liu and X. Tao, Biomacromolecules Enabled Dendrite-Free Lithium Metal Battery and Its Origin Revealed by Cryo-Electron Microscopy, *Nat. Commun.*, 2020,

11(1), 488, DOI: 10.1038/s41467-020-14358-1.

12. Z. Li, P. Qian, H. Li, H. Xiao, J. Chen and G. Li, Phosphorylated Cellulose Nanofibers Establishing Reliable Ion-Sieving Barriers for Durable Lithium-Sulfur Batteries, *J. Energy Chem.*, 2024, **92**, 619-628, DOI: 10.1016/j.jechem.2024.02.002.
13. C. Wang, W. Li, Y. Jin, J. Liu, H. Wang and Q. Zhang, Functional Separator Enabled by Covalent Organic Frameworks for High-Performance Li Metal Batteries, *Small*, 2023, **19**(28), 2300023, DOI: 10.1002/smll.202300023.
14. Y. Deng, A. Hussain, W. Raza, L. Ao, K. Zong, J. Zhao, W. Liu, P. Ye, A. Ramiere, X. Cai, D. Liu and J. Shen, Morphological Modulation of the PBI Membrane and Performance Optimization for Li-Metal Battery, *Chem. Eng. J.*, 2023, **474**, 145800, DOI: 10.1016/j.cej.2023.145800.
15. Y. Deng, A. Hussain, W. Raza, X. Cai, D. Liu and J. Shen, Review on Current Development of Polybenzimidazole Membrane for Lithium Battery, *J. Energy Chem.*, 2024, **91**, 579-608, DOI: 10.1016/j.jechem.2023.12.044.
16. D. Guo, L. Mu, F. Lin and G. Liu, Mesoporous Polyimide Thin Films as Dendrite-Suppressing Separators for Lithium–Metal Batteries, *ACS Nano*, 2024, **18**(1), 155-163, DOI: 10.1021/acsnano.3c04159.
17. J. P. Lowen, T. Insinna, T. V. Beatriceveena, M. P. Stockham, B. Dong, S. J. Day, C. P. Grey, E. Kendrick, P. R. Slater, P. A. Anderson and J. W. Makepeace, Probing the Electrochemical Behaviour of Lithium Imide as an Electrolyte for Solid-State Batteries, *EES Batteries*, 2025, **1**(3), 527-540, DOI: 10.1039/D5EB00058K.
18. J. Li, G. Li, R. Wang, Q. He, W. Liu, C. Hu, H. Zhang, J. Hui and F. Huo, Boron-Doped Dinickel Phosphide to Enhance Polysulfide Conversion and Suppress Shuttling in Lithium–Sulfur Batteries, *ACS Nano*, 2024, **18**(27), 17774-17785, DOI: 10.1021/acsnano.4c03315.
19. C. Zhou, M. Hong, N. Hu, J. Yang, W. Zhu, L. Kong and M. Li, Bi-Metallic Coupling-Induced Electronic-State Modulation of Metal Phosphides for Kinetics-Enhanced and Dendrite-Free Li–S Batteries, *Adv. Funct. Mater.*, 2023, **33**(14), 2213310, DOI: 10.1002/adfm.202213310.
20. B. Yuan, Y. Feng, X. Qiu, Y. He, L. Dong, S. Zhong, J. Liu, Y. Liang, Y. Liu, H. Xie, Z. Liu, J. Han and W. He, A Safe Separator with Heat-Dispersing Channels for High-Rate Lithium-Ion Batteries, *Adv. Funct. Mater.*, 2024, **34**(9), 2308929, DOI: 10.1002/adfm.202308929.
21. J. Wang, K. Jia, J. Ma, Z. Liang, Z. Zhuang, Y. Zhao, B. Li, G. Zhou and H.M. Cheng, Sustainable Upcycling of Spent $LiCoO_2$ to an Ultra-Stable Battery Cathode at High Voltage, *Nat. Sustain.*, 2023, **6**(7), 797-805, DOI: 10.1038/s41893-023-01094-9.
22. Y. He, Y. Qiao, Z. Chang and H. Zhou, The Potential of Electrolyte Filled MOF Membranes as Ionic Sieves in Rechargeable Batteries, *Energy Environ. Sci.*, 2019, **12**(8), 2327-2344, DOI: 10.1039/C8EE03651A.
23. Y. Takahashi, Neutron Structure Analysis of Poly(pyridobisimidazole) (PIPD), *Macromolecules*, 2002, **35**(10), 3942-3945, DOI: 10.1021/ma0121520.
24. J. C. L. Hageman, G. A. de Wijs, R. A. de Groot and E. A. Klop, The Role of the Hydrogen Bonding Network for the Shear Modulus of PIPD, *Polymer*, 2005, **46**(21), 9144-9154, DOI: 10.1016/j.polymer.2005.07.027.

25. A. Pogoreltsev, Y. Tulchinsky, N. Fridman and M. Gandelman, Nitrogen Lewis Acids, *JACS*, 2017, **139**(11), 4062-4067, DOI: 10.1021/jacs.6b12360.
26. X. Hao, J. Zhu, X. Jiang, H. Wu, J. Qiao, W. Sun, Z. Wang and K. Sun, Ultrastrong Polyoxyzole Nanofiber Membranes for Dendrite-Proof and Heat-Resistant Battery Separators, *Nano Lett.*, 2016, **16**(5), 2981-2987, DOI: 10.1021/acs.nanolett.5b05133.
27. Y. Takahashi, Crystal Structure of Poly(pyridobisimidazole), PIPD, *Macromolecules*, 2003, **36**(23), 8652-8655, DOI: 10.1021/ma030289f.
28. E. A. Klop and M. Lammers, XRD Study of the New Rigid-Rod Polymer Fibre PIPD, *Polymer*, 1998, **39**(24), 5987-5998, DOI: 10.1016/s0032-3861(97)10187-2.
29. N. Taloub, L. Liu, J. Li, N. Rahoui, Y. Huang and M. Hegazy, 3D Coating Layers of Polyhydroquinone Di-imidazopyridine (PIPD) Fibers to Improve Their Mechanical, Interfacial and Antimicrobial Properties, *Mater. Chem. Phys.*, 2021, **273**, 125124, DOI: 10.1016/j.matchemphys.2021.125124.
30. B. Athokpam, S.G. Ramesh and R.H. McKenzie, Effect of Hydrogen Bonding on the Infrared Absorption Intensity of OH Stretch Vibrations, *Chem. Phys.*, 2017, **488-489**, 43-54, DOI: 10.1016/j.chemphys.2017.03.006.
31. P.K. Deshmukh, K.P. Ramani, S.S. Singh, A.R. Tekade, V.K. Chatap, G.B. Patil and S.B. Bari, Stimuli-Sensitive Layer-by-Layer (LbL) Self-Assembly Systems: Targeting and Biosensory Applications, *J. Control. Release*, 2013, **166**(3), 294-306, DOI: 10.1016/j.jconrel.2012.12.033.
32. N. Taloub, L. Liu, N. Rahoui, M. Hegazy and Y. Huang, Grafting Multi-Walled Carbon Nanotubes (MWCNTs) into PIPD Fiber for Enhancing Mechanical and Interfacial Performance, *Polym. Test.*, 2019, **75**, 344-349, DOI: 10.1016/j.polymertesting.2019.02.016.
33. J. Sirichaisit and R. J. Young, Tensile and Compressive Deformation of Polypyridobisimidazole (PIPD)-Based 'M5' Rigid-Rod Polymer Fibres, *Polymer*, 1999, **40**(12), 3421-3431, DOI: 10.1016/s0032-3861(98)00561-8.
34. K. Wang, J. Duan, X. Chen, J. Wang, J. Li, L. Jiang, W. Yan, W. Lyu and Y. Liao, Nanofibrous Covalent Organic Frameworks Based Hierarchical Porous Separators for Fast-Charging and Thermally Stable Lithium Metal Batteries, *Adv. Energy Mater.*, 2024, **14**(25), 2401146, DOI: 10.1002/aenm.202401146.
35. T. Wang, Q. Liu, J. Zhou, X. Wang and B. Lu, Natural Supra-Molecular Structure Engineering for High-Performance Potassium Batteries Separator, *Adv. Energy Mater.*, 2022, **12**(44), 2202357, DOI: 10.1002/aenm.202202357.
36. H. Li, D. Wu, J. Wu, L.Y. Dong, Y.J. Zhu and X. Hu, Flexible, High-Wettability and Fire-Resistant Separators Based on Hydroxyapatite Nanowires for Advanced Lithium-Ion Batteries, *Adv. Mater.*, 2017, **29**(44), 1703548, DOI: 10.1002/adma.201703548.
37. X. Li, J. Zhang, X. Guo, C. Peng, K. Song, Z. Zhang, L. Ding, C. Liu, W. Chen and S. Dou, An Ultrathin Nonporous Polymer Separator Regulates Na Transfer toward Dendrite-Free Sodium Storage Batteries, *Adv. Mater.*, 2023, **35**(15), 2203547, DOI: 10.1002/adma.202203547.
38. L. Zuo, Q. Ma, P. Xiao, Q. Guo, W. Xie, D. Lu, X. Yun, C. Zheng and Y. Chen, Upgrading the Separators Integrated with Desolvation and Selective Deposition toward the Stable Lithium Metal Batteries, *Adv. Mater.*, 2024, **36**(13), 2311529, DOI:

View Article Online
DOI: 10.1039/D5EB00085H

10.1002/adma.202311529.

39. J. Dai, C. Shi, C. Li, X. Shen, L. Peng, D. Wu, D. Sun, P. Zhang and J. Zhao, A Rational Design of Separator with Substantially Enhanced Thermal Features for Lithium-Ion Batteries by the Polydopamine–Ceramic Composite Modification of Polyolefin Membranes, *Energy Environ. Sci.*, 2016, **9**(10), 3252-3261, DOI: 10.1039/C6EE01219A.
40. Y. Ji, L. Dong, J. Liu, H. Xie, S. Zhong, C. Yang, J. Han and W. He, A Li^+-Flux-Homogenizing Separator for Long-term Cycling of Li Metal Anodes, *Energy Environ. Sci.*, 2024, **17**(12), 4078-4089, DOI: 10.1039/D4EE00115J.
41. H. Lu, A. Du, X. Lin, Z. Zhang, S. Liu, Y. Xie, W. Li, J. Song, Y. Lu, W. Chen, C. Yang and Q.H. Yang, Rationally Coupling Thermal Tolerance, Thermal Conductance, and Overheating-Response in a Separator for Safe Batteries, *Energy Environ. Sci.*, 2024, **17**(20), 7860-7869, DOI: 10.1039/D4EE02302A.
42. J. Qian, Q. Chen, M. Hong, W. Xie, S. Jing, Y. Bao, G. Chen, Z. Pang, L. Hu and T. Li, Toward Stretchable Batteries: 3D-printed Deformable Electrodes and Separator Enabled by Nanocellulose, *Mater. Today*, 2022, **54**, 18-26, DOI: 10.1016/j.mattod.2022.02.015.
43. Z. Zou, M. Yin, P. Yin, Z. Hu, D. Wang and H. Pu, Facile Preparation of Surface-Modified Polypropylene Nanofiber Separators with Enhanced Ionic Transport and Welding Performance for Lithium-Ion Batteries, *Nano Energy*, 2024, **127**, 109774, DOI: 10.1016/j.nanoen.2024.109774.
44. Y.H. Liu, L.X. Li, A.Y. Wen, F.F. Cao and H. Ye, A Janus MXene/MOF Separator for the All-In-One Enhancement of Lithium-Sulfur Batteries, *Energy Stor. Mater.*, 2023, **55**, 652-659, DOI: 10.1016/j.ensm.2022.12.028.
45. C. Yuan, X. Yang, P. Zeng, J. Mao, K. Dai, L. Zhang and X. Sun, Recent Progress of Functional Separators with Catalytic Effects for High-Performance Lithium-Sulfur Batteries, *Nano Energy*, 2021, **84**, 105928, DOI: 10.1016/j.nanoen.2021.105928.
46. Q. Jin, K. Zhao, L. Wu, L. Li, L. Kong and X. Zhang, Enhancing Li Cycling Coulombic Efficiency while Mitigating "Shuttle Effect" of Li-S Battery through Sustained Release of $LiNO_3$, *J. Energy Chem.*, 2023, **84**, 22-29, DOI: 10.1016/j.jechem.2023.05.020.
47. Y. Wen, J. Ding, J. Liu, M. Zhu and R. Hu, A Separator Rich in SnF_2 and NO_3^- Directs an Ultra-Stable Interface toward High Performance Li Metal Batteries, *Energy Environ. Sci.*, 2023, **16**(7), 2957-2967, DOI: 10.1039/d3ee00664f.
48. D. Han, X. Wang, Y.N. Zhou, J. Zhang, Z. Liu, Z. Xiao, J. Zhou, Z. Wang, J. Zheng, Z. Jia, B. Tian, J. Xie, Z. Liu and W. Tang, A Graphene-Coated Thermal Conductive Separator to Eliminate the Dendrite-Induced Local Hotspots for Stable Lithium Cycling, *Adv. Energy Mater.*, 2022, **12**(25), 2201190, DOI: 10.1002/aenm.202201190.
49. J. Wu, H. Zeng, X. Li, X. Xiang, Y. Liao, Z. Xue, Y. Ye and X. Xie, Ultralight Layer-by-Layer Self-Assembled MoS_2-Polymer Modified Separator for Simultaneously Trapping Polysulfides and Suppressing Lithium Dendrites, *Adv. Energy Mater.*, 2018, **8**(35), 1802430, DOI: 10.1002/aenm.201802430.
50. J. Liu, J. Wang, L. Zhu, X. Chen, G. Yi, Q. Ma, S. Sun, N. Wang, X. Cui, Q. Chai, J. Feng and W. Yan, In Situ Grown MOFs and PVDF-HFP Co-Modified Aramid Gel Nanofiber Separator for High-Safety Lithium–Sulfur Batteries, *J. Mater. Chem. A*,

View Article Online
DOI: 10.1039/D5EB00085H

2022, **10**(26), 14098-14110, DOI: 10.1039/D2TA03301A.

51. M. Kim, S.Y. Hong, J. Bang and S.S. Lee, Highly Sustainable Polyphenylene Sulfide Membrane of Tailored Porous Architecture for High-performance Lithium-Ion Battery Applications, *Mater. Today Adv.*, 2021, **12**, 100186, DOI: 10.1016/j.mtadv.2021.100186.
52. J. Tan, J. Matz, P. Dong, J. Shen and M. Ye, A Growing Appreciation for the Role of LiF in the Solid Electrolyte Interphase, *Adv. Energy Mater.*, 2021, **11**(16), 2100046, DOI: 10.1002/aenm.202100046.
53. X. Dai, G. Lv, Z. Wu, X. Wang, Y. Liu, J. Sun, Q. Wang, X. Xiong, Y. Liu, C. Zhang, S. Xin, Y. Chen and T. Zhou, Flexible Hierarchical Co-Doped NiS_2@CNF-CNT Electron Deficient Interlayer with Grass-Roots Structure for Li–S Batteries, *Adv. Energy Mater.*, 2023, **13**(21), 2300452, DOI: 10.1002/aenm.202300452.
54. Z. Qiao, Y. Zhang, Z. Meng, Q. Xie, L. Lin, H. Zheng, B. Sa, J. Lin, L. Wang and D.L. Peng, Anchoring Polysulfides and Accelerating Redox Reaction Enabled by Fe-Based Compounds in Lithium–Sulfur Batteries, *Adv. Funct. Mater.*, 2021, **31**(21), 2100970, DOI: 10.1002/adfm.202100970.
55. C. Fan, R. Yang, Y. Huang, L. Mao, Y. Yang, L. Gong, X. Dong, Y. Yan, Y. Zou, L. Zhong and Y. Xu, Graphene Quantum Dots as Sulfiphilic and Lithiophilic Mediator toward High Stability and Durable Life Lithium-Sulfur Batteries, *J. Energy Chem.*, 2023, **85**, 254-266, DOI: 10.1016/j.jechem.2023.06.030.
56. Z. Li, Y. Sun, X. Wu, H. Yuan, Y. Yu and Y. Tan, Boosting Adsorption and Catalysis of Polysulfides by Multifunctional Separator for Lithium–Sulfur Batteries, *ACS Energy Lett.*, 2022, **7**(12), 4190-4197, DOI: 10.1021/acsenergylett.2c02232.
57. S. Hu, M. Yi, X. Huang, D. Wu, B. Lu, T. Wang, N. Li, Z. Zhu, X. Liu and J. Zhang, Cobalt-Doped Porphyrin-Based Porous Organic Polymer-Modified Separator for High-Performance Lithium–Sulfur Batteries, *J. Mater. Chem. A*, 2021, **9**(5), 2792-2805, DOI: 10.1039/D0TA10607K.
58. H. Duan, K. Li, M. Xie, J.M. Chen, H.G. Zhou, X. Wu, G.H. Ning, A. I. Cooper and D. Li, Scalable Synthesis of Ultrathin Polyimide Covalent Organic Framework Nanosheets for High-Performance Lithium–Sulfur Batteries, *JACS*, 2021, **143**(46), 19446-19453, DOI: 10.1021/jacs.1c08675.
59. H. Pei, X. Guan, X. Chen, Y. Chen, Y. Yang, Y. Wen, H. Nie, L. Chang, X. Zhou, X. Xie, L. Ye and Y.W. Mai, Multifunctional Tri-Layer Aramid Nanofiber Composite Separators for High-Energy-Density Lithium-Sulfur Batteries, *Nano Energy*, 2024, **126**, 109680, DOI: 10.1016/j.nanoen.2024.109680.
60. C. Sun, J. Sheng, Q. Zhang, R. Gao, Z. Han, C. Li, X. Xiao, L. Qiu and G. Zhou, Self-Extinguishing Janus Separator with High Safety for Flexible Lithium-Sulfur Batteries, *Sci. China Mater.*, 2022, **65**(8), 2169-2178, DOI: 10.1007/s40843-022-2034-5.

View Article Online
DOI: 10.1039/D5EB00085H

Data Availability Statement

The data that support the findings of this article are available from the corresponding author upon reasonable request.